

Probing a Local Viscosity Change at the Nematic-Isotropic Liquid Crystal Phase Transition by a Ratiometric Flapping Fluorophore

Ryo Kimura,^a Hidetsugu Kitakado,^a Takuya Yamakado,^a Hiroyuki Yoshida,^{*b} and Shohei Saito^{*a}

^aGraduate School of Science, Kyoto University, Kitashirakawa Oiwake, Sakyo, Kyoto 606-8502, Japan.

^bGraduate School of Engineering, Osaka University, 2-1 Yamadaoka, Suita, Osaka 565-0871, Japan

Local viscosity change in the thermal phase transition of a nematic liquid crystal, 5CB, has been analyzed by doping fluorescent viscosity probes, flapping fluorophores (FLAP) as well as a molecular rotor BODIPY-C₁₂. As a result, only flapping anthraceneimide has successfully monitored a small viscosity change (corresponding to a few cP (centipoise) change in shear viscosity around 25 cP) in the nematic-to-isotropic phase transition by ratiometric spectroscopy. In addition, analysis of fluorescence anisotropy indicates that the emissive species (planarized flapping anthraceneimides) are aligned parallel to the director of 5CB in the nematic phase.

Analysis of the viscosity of liquid crystals is important not only in basic science^[1] but also in applications to displays and microfluidic devices^[2]. Since low-viscosity nematic liquid crystals have a fast response time to external fields, molecular theory to describe the viscosity of nematic liquid crystals have been widely discussed.^[3] 5CB (4-cyano-4'-pentylbiphenyl) is one of the most-studied nematic liquid crystal, which shows a thermal phase transition at the clearing point around 35 °C. A discontinuous decrease in shear viscosity (only by a few cP change around 25 cP) during the isotropic-to-nematic phase transition of 5CB was reported using a rheometer (Fig. 1a) and discussed along with a small discontinuous increase in density.^[4] However, it is challenging to monitor "local viscosity" in a phase transition of LC materials by using fluorescent molecular viscosity probes. Although one example was reported for a fluorogenic molecular rotor to detect a phase transition of a liquid crystal "80B4100", the structure, phase and viscosity value of this liquid crystal were undisclosed.^[5] Local viscosity is a different measure from shear viscosity obtained from rheometers. Local viscosity reflects the degree to which ultrafast conformational dynamics of photoexcited molecules is suppressed in a nanoscale environment. While molecular viscosity probes represented by molecular rotors have been widely used for bioimaging technique,^[6] applications to monitoring nano-environments of condensed matter have been also demonstrated.^[7,8a]

With this background, we have previously developed flapping fluorophores (FLAP) as a new category of molecular viscosity probe.^[8] While conventional molecular rotors probe local viscosity by internal rotation dynamics, the flapping fluorophores sense nano-environments by a bent-to-planar conformational change in the excited state. The flapping fluorophores show high sensitivity particularly in a low viscosity range below 100 cP.^[8a,8c-e] Very recently, a modified flapping

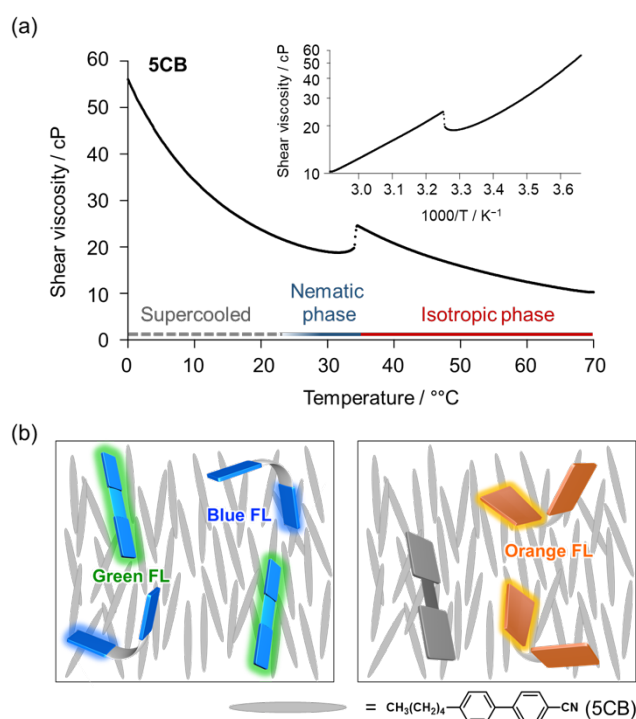


Fig. 1. (a) Temperature-dependent shear viscosity of 5CB, measured in a cooling process (6 °C/min) by a rheometer. (inset) Andrade plot (b) Schematic representation of a nematic liquid crystal doped with viscosity-probing flapping fluorophores **FLAP0** (ratiometric probe; left) and **FLAP1** (fluorogenic probe; right), in which photoexcited molecules are partially planarized.

probe even realized real-time monitoring of dynamic polymer free volume by single-molecule fluorescence spectroscopy.^[8f] Here, we report the attempts to monitor the local viscosity change in the thermal phase transition of 5CB, using flapping fluorophores (Fig. 1b) as well as a commonly-used molecular rotor, **BODIPY-C₁₂**.^[6a,9] Furthermore, we have analyzed anisotropy in the absorption/fluorescence of the FLAP-doped 5CB with uniaxial alignment to gain insight into the orientation of the FLAP molecules in a liquid crystal.

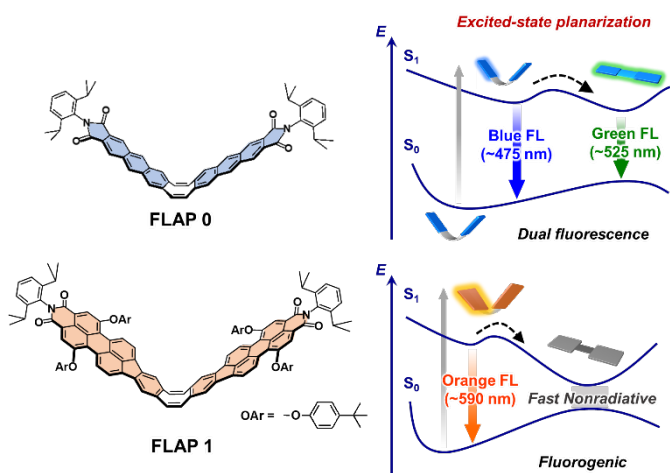


Fig. 2. Flapping anthraceneimide **FLAPO** and flapping peryleneimide **FLAP1** (left). Dual fluorescence properties of **FLAPO** and fluorogenic properties of **FLAP1** are demonstrated with their energy profiles of the ground state (S_0) and the excited state (S_1) (right).

FLAPO^[8a-8c] and **FLAP1**^[8d,8e] were synthesized according to the reported protocols. Since their planarization dynamics and an accompanying electronic configurational switch in S_1 are sensitive to local environments, both **FLAPO** and **FLAP1** work as a viscosity probe in a low viscosity range (below 100 cP). However, a subtle difference in their S_1 excited state profiles leads to the distinct spectroscopic responses. **FLAPO** shows a bright green FL emitted from the planar geometry (Fig. S4-5) in low-viscosity media, while the intensity of the blue fluorescence (FL) derived from the V-shaped geometry (Fig. S4-4) increases in high-viscosity media due to the suppression of the planarization in the excited state.^[8a] Polarity-independence has also been confirmed in the ratiometric FL of **FLAPO**. On the contrary, **FLAP1** does not show FL from the planar geometry due to fast nonradiative decay. However, the S_1 conformational planarization of **FLAP1** is significantly suppressed by increasing viscosity, and it works as a fluorogenic viscosity probe. A pronounced FL enhancement and a prolonged FL lifetime are observed in a viscous media even less than 3 cP.^[8d,8e] BODIPY-C₁₂ is categorized as a fluorogenic molecular rotor. Since the dynamic internal rotation in S_1 is suppressed in highly viscous media, FL quantum yield increases with bright green FL and FL lifetime prolongs.^[6a,9]

We started experiments from FL measurements of the three molecular viscosity probes in 5CB (*ca.* 20-cP viscosity at 25 °C) and in benzonitrile (PhCN; 1.2-cP viscosity at 25 °C), which is a reference solvent bearing a similar dipole moment to 5CB (Fig. 3, See Chapter 1 in the SI for details). The ratiometric probe **FLAPO** shows a smaller FL ratio of I_{528}/I_{475} (= 3.9) in 5CB than in PhCN (9.2). This indicates that the planarization in S_1 is partially suppressed due to higher viscosity of 5CB and the blue fluorescence from the V-shaped conformer was observed more significantly. On the other hand, the fluorogenic probe **FLAP1** display a large difference in FL quantum yield and FL lifetime. In PhCN, the FL quantum yield (Φ_F) of **FLAP1** was 0.008 and the fluorescence lifetime (τ_F) was about 0.2 ns, whereas, in 5CB, Φ_F increased more than 10 times to 0.11 and τ_F also prolonged to 1.1 ns. The similar tendency was observed for BODIPY-C₁₂ (Φ_F = 0.056, τ_F = 0.62 ns in PhCN and Φ_F = 0.26, τ_F = 2.2 ns in 5CB). These results also indicate that the planarization of **FLAP1** as well as the internal bond rotation of BODIPY-C₁₂ is partially

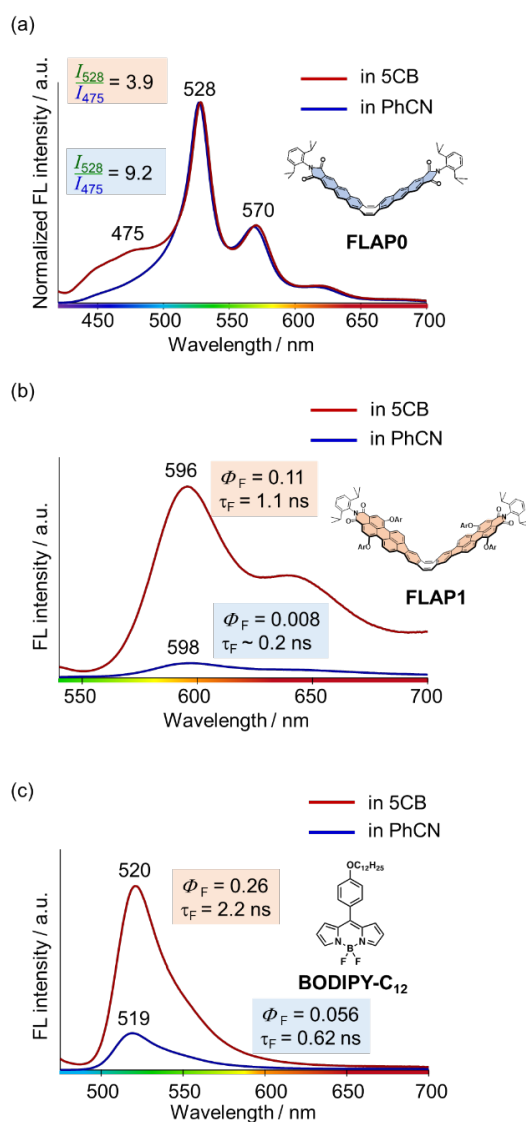


Fig. 3. FL properties of (a) **FLAPO** (λ_{ex} = 405 nm), (b) **FLAP1** (λ_{ex} = 520 nm), and (c) BODIPY-C₁₂ (λ_{ex} = 460 nm) in 5CB and in PhCN. Concentration of the viscosity probes 10^{-4} M. Non-polarized excitation with no analyzer in a standard quartz cuvette (1.0 mm).

suppressed in viscous 5CB. In other words, the difference of local viscosity between PhCN and 5CB was detectable with all three probes.

Next, temperature dependence of the FL properties was studied in 5CB (Fig. 4). The concentration of the fluorescent probes is in the order of 10^{-5} M (less than 10^{-2} wt%), which has no influence on the thermal phase transition of 5CB (Fig. S2-7). As the temperature increased over the clearing point of 5CB (isotropic phase), the FL ratio of I_{528}/I_{475} continuously increased in **FLAPO**, and the fluorescence lifetime became shorter in **FLAP1**. On the other hand, a rigid peryleneimide fluorophore **Wing1**, which is a reference compound of flexible **FLAP1**, showed almost constant FL lifetime in the higher temperature range (Fig. S2-5). These results clearly indicate that the observed FL responses of FLAP are derived from the flexible motion, and that the planarization dynamics in S_1 is promoted in higher temperature. BODIPY-C₁₂ also showed the similar

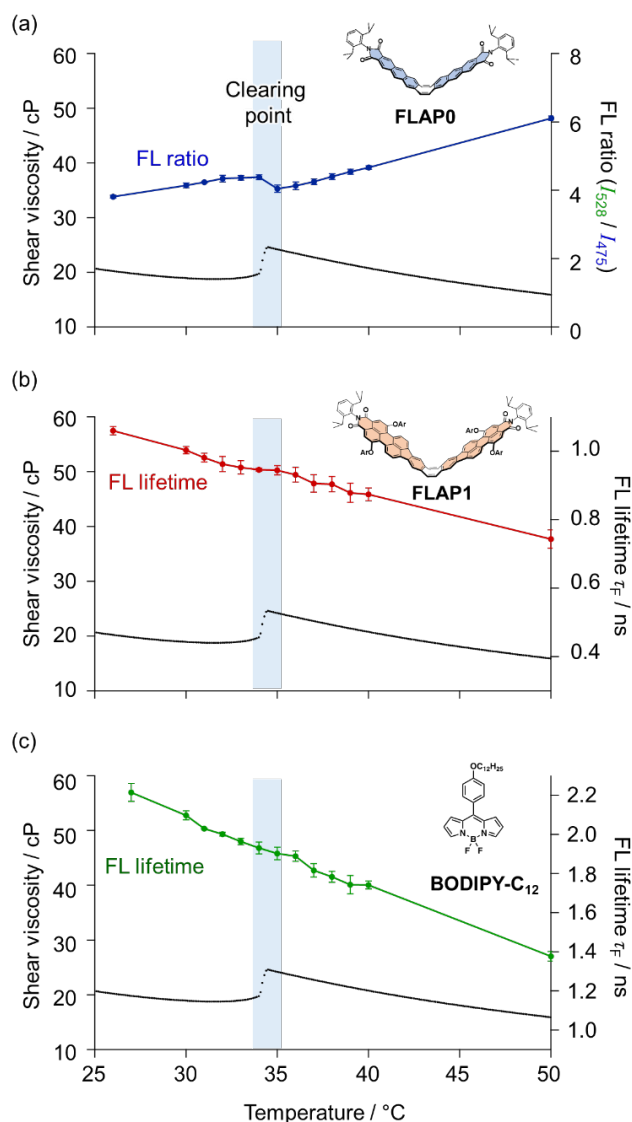


Fig. 4. Temperature-dependent (a) FL ratio of **FLAPO**, (b) FL lifetime of **FLAP1**, and (c) FL lifetime of **BODIPY-C₁₂** doped in 5CB. Each measurement was performed when the temperature remains constant for 5–10 min after the gradual heating. Measurements were performed 3 times to display sample standard deviation.

tendency with **FLAP1**. Interestingly, these tendencies of the three probes are also consistent in the temperature range below the clearing point (nematic phase). However, more importantly, only **FLAPO** displayed a characteristic discontinuous change in the I_{528}/I_{475} FL ratio at the nematic-to-isotropic phase transition of 5CB, whereas **FLAP1** and **BODIPY-C₁₂** did not detect the phase transition by the FL lifetime measurement. The values of the FL ratio (I_{528}/I_{475}) using **FLAPO** was 4.4 ± 0.1 at 34 °C and 4.0 ± 0.1 at 35 °C. The significant decrease of the FL ratio over the narrow temperature range can be attributed to the detection of a nano-environmental change by the phase transition. Since **FLAPO** has the polarity independence in a wide range of dielectric permittivities,^[8a,8c] the decrease of the FL ratio can be mainly assigned to the increase in "local viscosity" around the clearing point in the nematic-to-isotropic phase transition. Namely, the

planarization dynamics of **FLAPO** in the excited state become slightly more suppressed when the nematic 5CB turns isotropic at the clearing point. It is noteworthy that the shear viscosity measured by a rheometer also increased in the nematic-to-isotropic phase transition. The agreement supports the close relationship between the macroscopic and microscopic (local) viscosities, which has been recognized as Förster–Hoffman (F-H) equation (Fig. S2-4),^[6a,6b,9] particularly in Newtonian fluids. The efficacy of **FLAPO** over **BODIPY-C₁₂** for the detection of the phase transition would originate from the different motions for the viscosity sensing (flapping vs rotation) and the gap of the required free volumes for the dynamic conformational change.^[8f] On the other hand, the unsuccessful detection by **FLAP1** would be simply due to the saturated viscosity response below 20 cP.^[8e]

Anisotropy in the absorption/FL of **FLAPO** in a uniaxially aligned 5CB was investigated by micro-spectroscopy to gain insight into the molecular orientation of **FLAPO** in the liquid crystal host (see Fig. S3-1 for details of the measurement). Here, **FLAPO** was doped in 5CB at a weight ratio of 0.5 wt% or 1 wt%, and the mixture was filled in a glass sandwich cell with uniaxial rubbing treatment. Measurement of polarized absorbance spectra showed a small anisotropy along the LC director that disappeared in the isotropic phase (Fig. S3-2), indicating that the orientation of the V-shaped **FLAPO** molecules is not isotropic in the ground state (See the transition dipoles in Fig. S4-2). Upon non-polarized excitation at approx. 380 nm, the emission was anisotropic with stronger intensity along the director, and interestingly, the intensity ratio of the emission peaks (FL ratio) varied depending on polarization (Fig. 5, Fig. S3-3). Whereas the blue emission peak at 475 nm, attributed to the V-shaped **FLAPO**, showed a fluorescent dichroic ratio of $I_{//}/I_{\perp} = 1.6$, the green emission peak at 528 nm, attributed to the planarized **FLAPO**, showed a larger value of $I_{//}/I_{\perp} = 2.5$, causing the I_{528}/I_{475} intensity ratio to vary between 1.8 and 1.2. The anisotropy disappeared in the isotropic phase (Fig. S3-4), suggesting that the nematic order causes the planarization of **FLAPO** to occur preferentially along the nematic director. In fact, it is well known that the viscosity of liquid crystals is anisotropic and depends on the relative directions of the director^[3]; it is therefore natural for the "local viscosity" to also be anisotropic and depend on the relative orientations of the fluorescent probe and the director. Measurement of the non-polarized fluorescence spectrum upon polarized excitation also supported the anisotropy in planarization probability, giving a larger I_{528}/I_{475} ratio for excitation polarized along the director (Fig. S3-5). Since the planarization rate of **FLAPO** is much faster (subnanoseconds in its time constant) than the spectral acquisition rate in these measurements, further investigation employing ultrafast pump-probe experiments^[10] as well as molecular dynamics (MD) simulations would be necessary to fully understand the orientation dynamics of **FLAPO** in a liquid crystal. Nevertheless, their capability for ratiometric detection of small viscosity changes at the nematic-isotropic phase transition, which was also confirmed from microscopic measurements (Fig. S3-6), make flapping fluorophores promising candidates where other probes fall short.

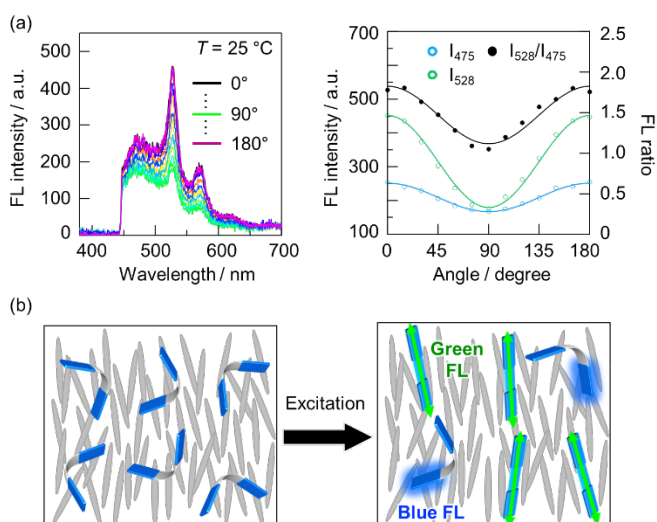


Fig. 5. (a) Analyzer-angle dependence in the FL spectra of **FLAPO** doped in 5CB at 25 °C (nematic phase, uniaxial alignment) (left). Non-polarized excitation: 380 nm. The FL intensities at 475 nm and 528 nm, and the FL ratio of I_{528}/I_{475} plotted with relative directions to the 5CB director (right). (b) Schematic representation of the anisotropic green fluorescence from the planarized excited species and the less anisotropic blue fluorescence from the V-shaped excited species.

Conclusion

Three molecular viscosity probes, a ratiometric flapping fluorophore **FLAPO**, a fluorogenic flapping fluorophore **FLAP1**, and a fluorogenic molecular motor **BODIPY-C₁₂** were doped in a nematic liquid crystal 5CB, and their fluorescence properties were analyzed at different temperatures. As a result, only by the ratiometric fluorescence spectroscopy using **FLAPO**, a small discontinuous viscosity gap (corresponding to a few cP change in shear viscosity around 20 cP) during the nematic-to-isotropic phase transition of 5CB was successfully detected. Moreover, planarized emissive species of **FLAPO** tend to be parallel to the director of 5CB. These results provide a deeper insight into the molecular theory of the liquid crystal viscosity and will lead to real-time 2D imaging technique of local viscosity during the phase transition of liquid crystals.

Acknowledgement

This work was supported by JST PRESTO (FRONTIER) and JST FOREST Grant Numbers JPMJPR16P6 (S.S.) and JPMJFR201L (S.S.), JSPS KAKENHI Grant Numbers JP21H01917 (S.S.), JP19H02581 (H.Y.) and JP20K21154 (H.Y.), MEXT LEADER Program (H.Y.), Toray Science Foundation (S.S.) and JSPS Research Fellowship for Young Scientists Grant Numbers JP21J22951 to R.K. and JP19J22034 to T. Y.

Conflicts of interest

There are no conflicts to declare.

References

1. P.-G. de Gennes and J. Prost, *The Physics of Liquid Crystals*, 2nd Ed, Clarendon Press, Oxford, **1993**.
2. (a) H. Chen, M. Hu, F. Peng, J. Li, Z. An and S.-T. Wu, *Optical Materials Express*, **2015**, *5*, 655; (b) S. Čopar, Ž. Kos, T. Emeršič, and U. Tkalec, *Nature Commun.* **2020**, *11*, 59.
3. (a) V. V. Beryaev, *Viscosity of Nematic Liquid Crystals*, Cambridge Intl. Science Pub., **2009**; (b) H. Kneppel, F. Schneider and N. K. Sharma, *J. Chem. Phys.*, **1982**, *77*, 3203; (c) A. G. Chmielewski, *Mol. Cryst. Liq. Cryst.*, **1986**, *132*, 339; (d) S.-T. Wu and C.-S. Wu, *Physical Review A*, **1990**, *42*, 2219.
4. R. Shimada, O. Urakawa, T. Inoue and H. Watanabe, *Soft Matter*, **2021**, *17*, 6259.
5. F. Zhou, J. Shao, Y. Yang, J. Zhao, H. Guo, X. Li, S. Ji and Z. Zhang, *Eur. J. Org. Chem.* **2011**, 4773.
6. (a) M. K. Kuimova, *Phys. Chem. Chem. Phys.* **2012**, *14*, 12671; (b) M. A. Haidekker and E. A. Theodorakis, *J. Mater. Chem. C* **2016**, *4*, 2707; (c) A. S. Klymchenko, *Acc. Chem. Res.*, **2017**, *50*, 366.
7. (a) H. Itagaki, K. Horie and I. Mita, *Prog. Polym. Sci.*, **1990**, *15*, 361; (b) B. Strehmel, V. Strehmel and M. Younes, *J. Polym. Sci., Part B: Polym. Phys.*, **1999**, *37*, 1367; (c) M. Aoki, D. Kawaguchi, T. Ganbe, N. Sekine, K. Okamoto and K. Tanaka, *Chem. Lett.* **2015**, *44*, 659.
8. (a) R. Kotani, H. Sotome, H. Okajima, S. Yokoyama, Y. Nakaïke, A. Kashiwagi, C. Mori, Y. Nakada, S. Yamaguchi, A. Osuka, A. Sakamoto, H. Miyasaka and S. Saito, *J. Mater. Chem. C* **2017**, *5*, 5248; (b) C. Yuan, S. Saito, C. Camacho, S. Irle, I. Hisaki and S. Yamaguchi, *J. Am. Chem. Soc.* **2013**, *135*, 8842; (c) W. Nakanishi, S. Saito, N. Sakamoto, A. Kashiwagi, S. Yamaguchi, H. Sakai and K. Ariga, *Chem. Asian J.* **2019**, *14*, 2869; (d) R. Kimura, H. Kuramochi, P. Liu, T. Yamakado, A. Osuka, T. Tahara and S. Saito, *Angew. Chem. Int. Ed.* **2020**, *59*, 16430; (e) R. Kimura, H. Kitakado, A. Osuka and S. Saito, *Bull. Chem. Soc. Jpn.* **2020**, *93*, 1102; (f) Y. Goto, S. Omagari, R. Sato, T. Yamakado, R. Achiwa, N. Dey, K. Suga, M. Vacha and S. Saito, *J. Am. Chem. Soc.* **2021**, *143*, 14306.
9. A. Polita, S. Toliautas, R. Žvirblis and A. Vyšiauska, *Phys. Chem. Chem. Phys.*, **2020**, *22*, 8296.
10. (a) M. Hada, S. Saito, S. Tanaka, R. Sato, M. Yoshimura, K. Mouri, K. Matsuo, S. Yamaguchi, M. Hara, Y. Hayashi, F. Röhrich, R. Herges, Y. Shigeta, K. Onda and R. J. Dwayne Miller, *J. Am. Chem. Soc.* **2017**, *139*, 15792; (b) M. Hada, D. Yamaguchi, T. Ishikawa, T. Sawa, K. Tsuruta, K. Ishikawa, S. Koshihara, Y. Hayashi and T. Kato, *Nat. Commun.* **2019**, *10*, 4159.

Supporting Information

Probing a Local Viscosity Change at the Nematic-Isotropic Liquid Crystal Phase Transition by a Ratiometric Flapping Fluorophore

Ryo Kimura,^a Hidetsugu Kitakado,^a Takuya Yamakado,^a Hiroyuki Yoshida,^{*b} and Shohei Saito^{*a}

^a Graduate School of Science, Kyoto University, Kitashirakawa Oiwake, Sakyo, Kyoto 606-8502, Japan

^b Graduate School of Engineering, Osaka University, 2-1 Yamadaoka, Suita, Osaka 565-0871, Japan

Corresponding Authors

yoshida@eei.eng.osaka-u.ac.jp

s_saito@kuchem.kyoto-u.ac.jp

Contents

1. General information.....	S2
2. Photophysical, rheological, and thermal analyses	S3–S12
3. Microscopic measurements	S13–S15
4. Density functional theory (DFT) calculations	S16–S20
5. Supporting references	S21

1. General information

Synthesis

All reagents and solvents were of commercial grade and were used without further purification unless otherwise noted. Benzonitrile (PhCN) was distilled before optical measurements. **FLAP0**^[S1], **FLAP1**^[S2], **Wing1**^[S2], and **BODIPY-C₁₂**^[S3] were synthesized according to the reported methods.

Measurements

All optical measurements were performed under air-saturated condition. In Chapter 2, excitation light and emissions were non-polarized. UV-visible absorption spectra were recorded on a Shimadzu UV-3600 spectrometer. Steady-state fluorescence and excitation spectra were recorded on a JASCO FP-8500 spectrofluorometer. Absolute fluorescence quantum yields were determined by an integrating sphere system on a HAMAMATSU C9920-02S apparatus. Fluorescence lifetimes were measured on a compact fluorescence lifetime spectrometer Hamamatsu Photonics QuantaaurusTau C11367. Optical measurements were conducted using a 1-cm square quartz cell in PhCN, and 1-mm quartz cell in 5CB. Measurements of temperature-dependent FL spectra and FL lifetimes were conducted on UNISOKU CoolSpeK connected with a JASCO FP-8500 or a Hamamatsu Photonics QuantaaurusTau C11367. Shear viscosity of 5CB was measured on an Anton Paar MCR702 rheometer. Differential scanning calorimetry (DSC) was recorded on a Hitachi High-Tech TA7000.

In Chapter 3, the optical set-up and measurement conditions were shown in the following Figures.

2. Photophysical, rheological, and thermal analyses

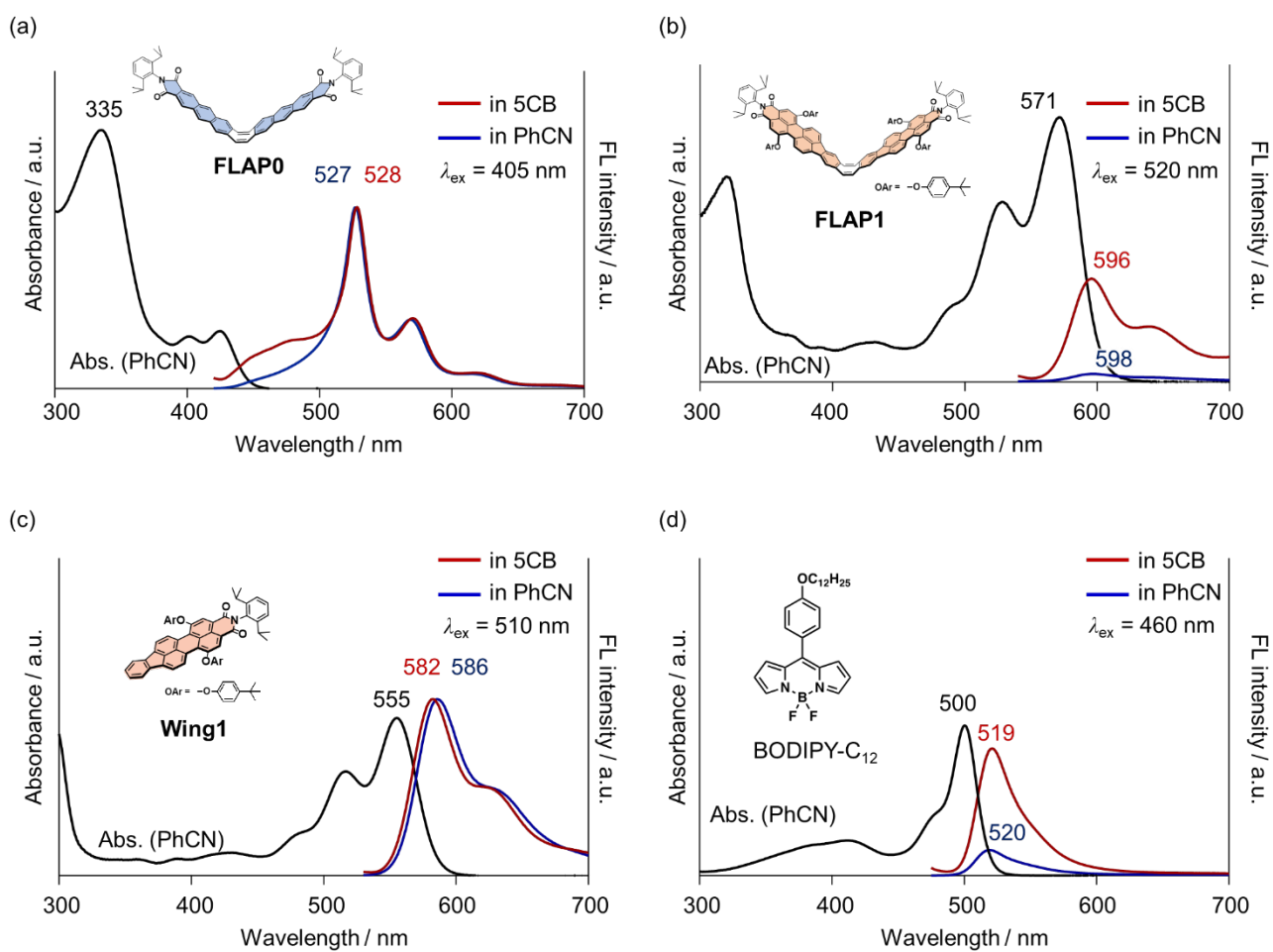


Figure S2-1. UV-visible absorption and FL spectra of (a) **FLAP0**, (b) **FLAP1**, (c) **Wing1**, and (d) **BODIPY-C₁₂** in PhCN and 5CB. Excitation wavelengths: 405 nm for **FLAP0**, 520 nm for **FLAP1**, 510 nm for **Wing1**, and 460 nm for **BODIPY-C₁₂**.

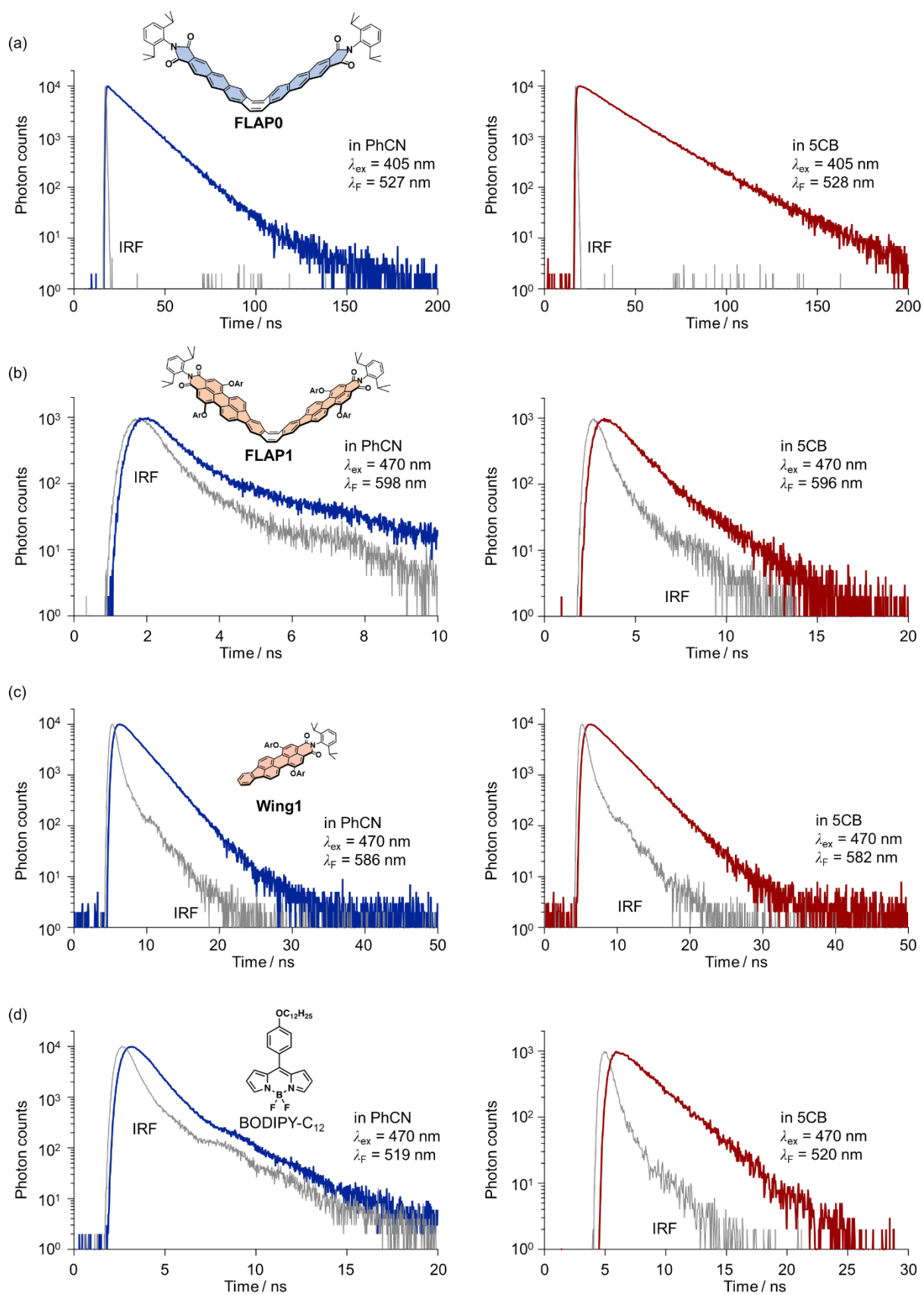


Figure S2-2. FL decay profiles of (a) FLAP0, (b) FLAP1, (c) Wing1, and (d) BODIPY-C₁₂ in PhCN (left) and 5CB (right). Excitation and fluorescence wavelengths are shown in each panel.

Table S2-1. FL quantum yield Φ_F and FL lifetime τ_F of **FLAP0**, **FLAP1**, **Wing1**, and BODIPY-C₁₂ in PhCN and 5CB.

Compounds	Solvents	Φ_F ^[a]	τ_{F1}	τ_{F2}	A_1	A_2	χ^2
FLAP0	PhCN	0.44	0.13 ns ^[b]	13 ns	-1840 ^[b]	2270	1.22
	5CB	0.48	0.62 ns ^[b]	20 ns	-1290 ^[b]	2440	1.68
FLAP1	PhCN	0.008	0.16 ns ^[b]	2.8 ns	64 ^[b]	1.0	1.25
	5CB	0.11	1.1 ns				1.22
Wing1	PhCN	0.37	2.2 ns				1.18
	5CB	0.46	2.6 ns				1.30
BODIPY-C ₁₂	PhCN	0.056	0.62 ns				1.42
	5CB	0.26	2.2 ns				1.29

[a] Excitation wavelengths for the determination of Φ_F : $\lambda_{ex} = 405$ nm (**FLAP0**), $\lambda_{ex} = 520$ nm (**FLAP1**), $\lambda_{ex} = 510$ nm (**Wing1**), and $\lambda_{ex} = 460$ nm (BODIPY-C₁₂).

[b] FL lifetime was fitted with $f(t) = A_1 \exp(-t/\tau_1) + A_2 \exp(-t/\tau_2)$. Short-lived components ($\tau_1 < 1$ ns) of **FLAP0** obtained as negative A_1 values would originate from planarization dynamics in the excited state.^[S2]

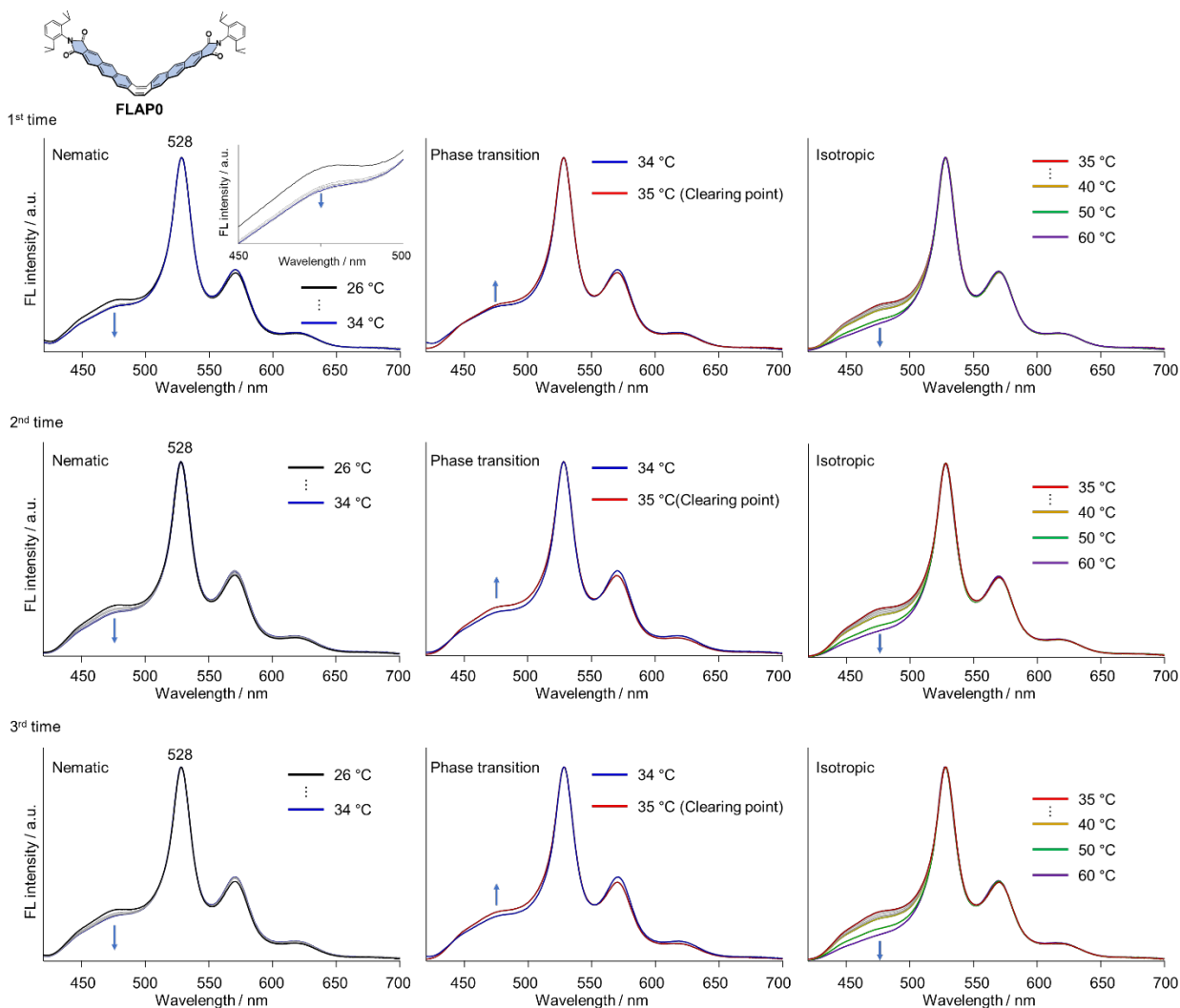


Figure S2-3. Temperature-dependent FL spectra of **FLAP0** in 5CB ($\lambda_{\text{ex}} = 405$ nm). The measurements were performed three times.

Table S2-2. Temperature-dependent FL ratio of **FLAP0** in 5CB ($\lambda_{\text{ex}} = 405$ nm) for the three measurements.

Temperature / °C	FL ratio (I_{528} / I_{475})			
	1 st	2 nd	3 rd	
Nematic	26	3.78	3.86	3.81
	30	4.22	4.11	4.10
	31	4.26	4.22	4.23
	32	4.29	4.45	4.28
	33	4.36	4.44	4.30
	34	4.34	4.47	4.34
Clearing point	35	4.16	4.01	3.96
Isotropic	36	4.25	4.11	4.03
	37	4.35	4.23	4.18
	38	4.50	4.36	4.34
	39	4.62	4.53	4.47
	40	4.71	4.68	4.61
	50	6.14	6.15	6.03
60	7.00	7.37	7.45	

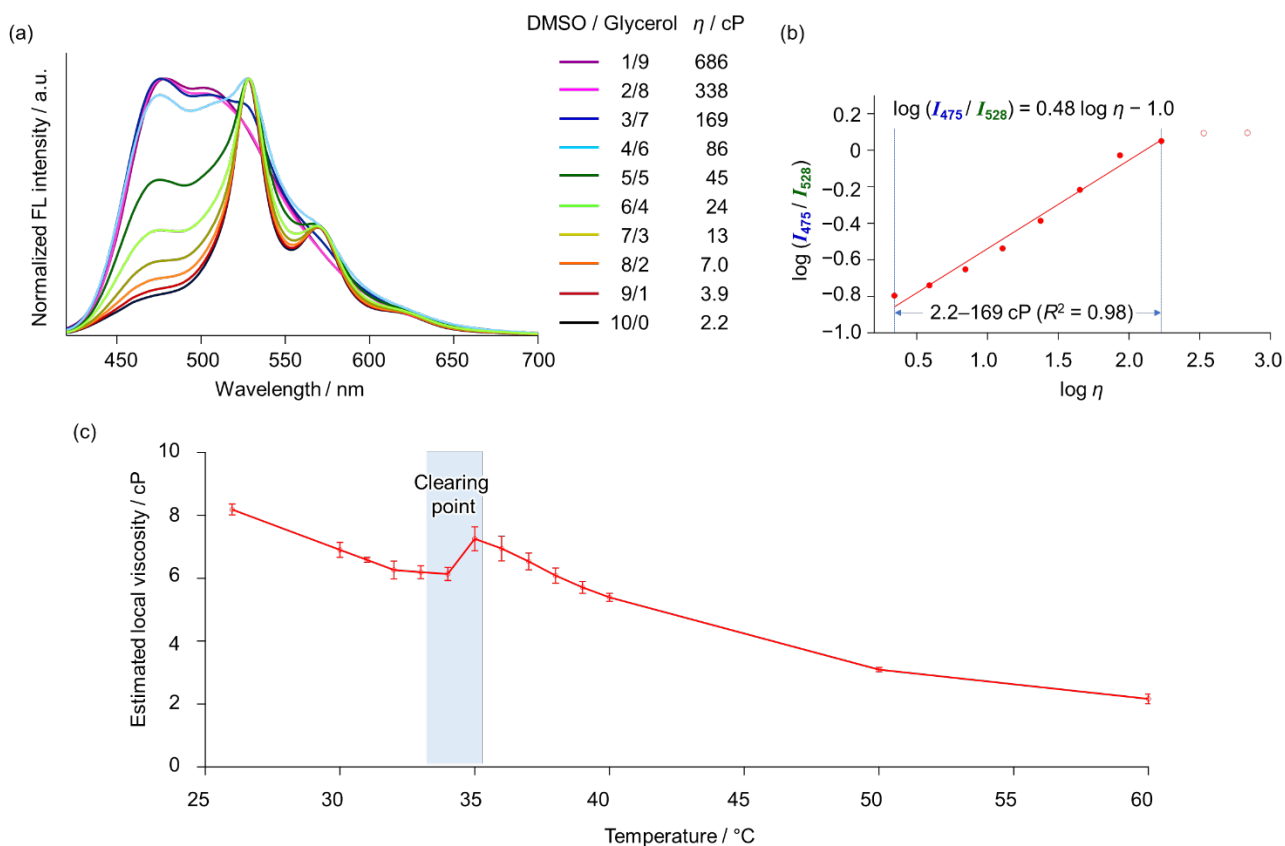


Figure S2-4. (a) Viscosity-dependent FL spectra of **FLAP0** in mixed solvents of DMSO/glycerol (v/v). Excitation by non-polarized light ($\lambda_{\text{ex}} = 405$ nm). (b) The corresponding Förster–Hoffman plot between 2.2 cP to 169 cP. (c) Local viscosity of 5CB at each temperature estimated from the Förster–Hoffman calibration of **FLAP0**. Measurements were performed 3 times to display sample standard deviation. The local viscosity of 5CB was formally estimated as 6.1 ± 0.2 cP at 34 °C and 7.3 ± 0.4 cP at 35 °C, although the anisotropy of the FL ratio (See Chapter 3) was not considered in these values.

Note: The previously reported Förster–Hoffman plot^[S4] was corrected as a double logarithmic graph from the same dual fluorescence spectra.

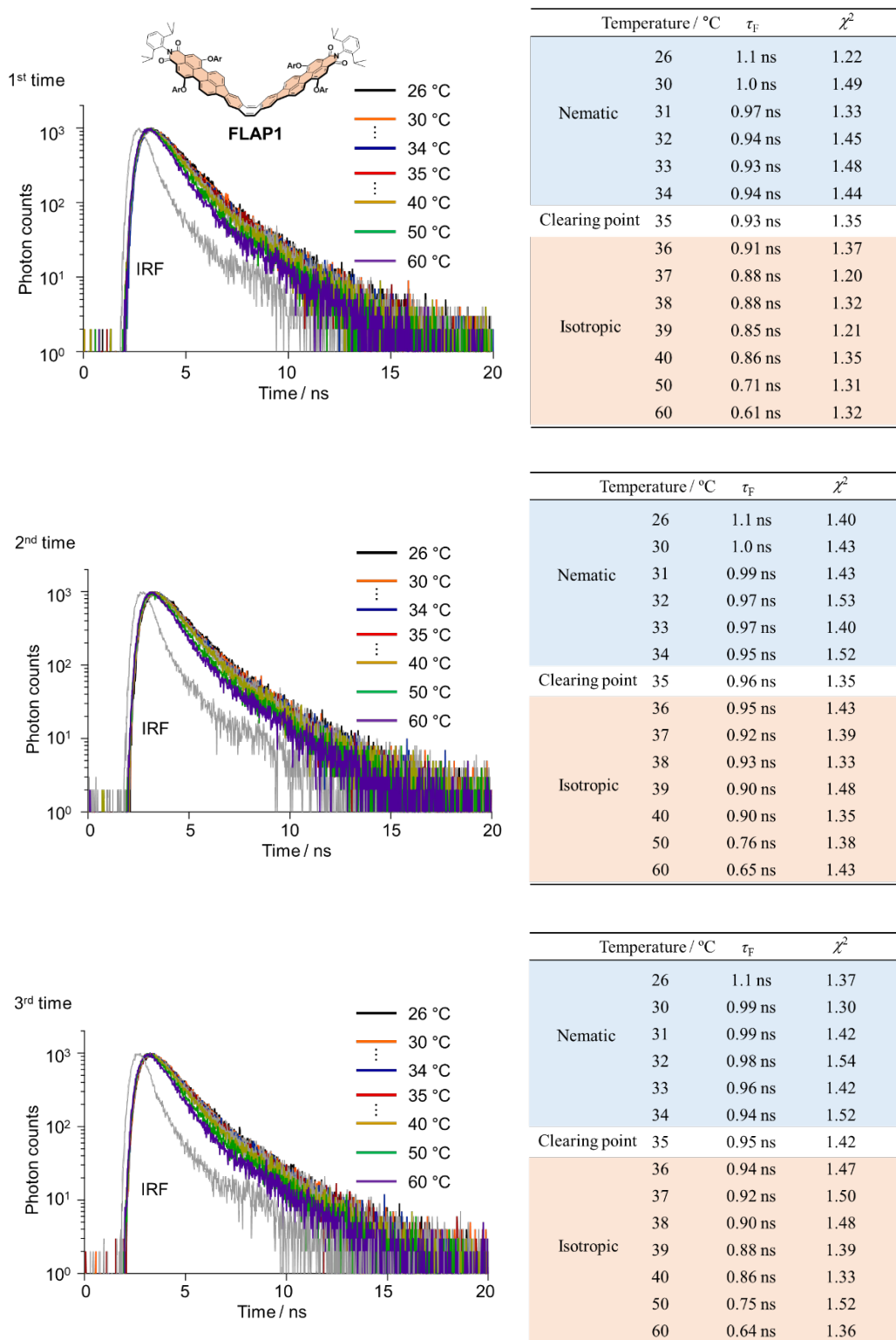


Figure S2-5. Temperature-dependent FL decay profiles and FL lifetimes of **FLAP1** in 5CB ($\lambda_{\text{ex}} = 470$ nm and $\lambda_{\text{F}} = 596$ nm) for three measurements.

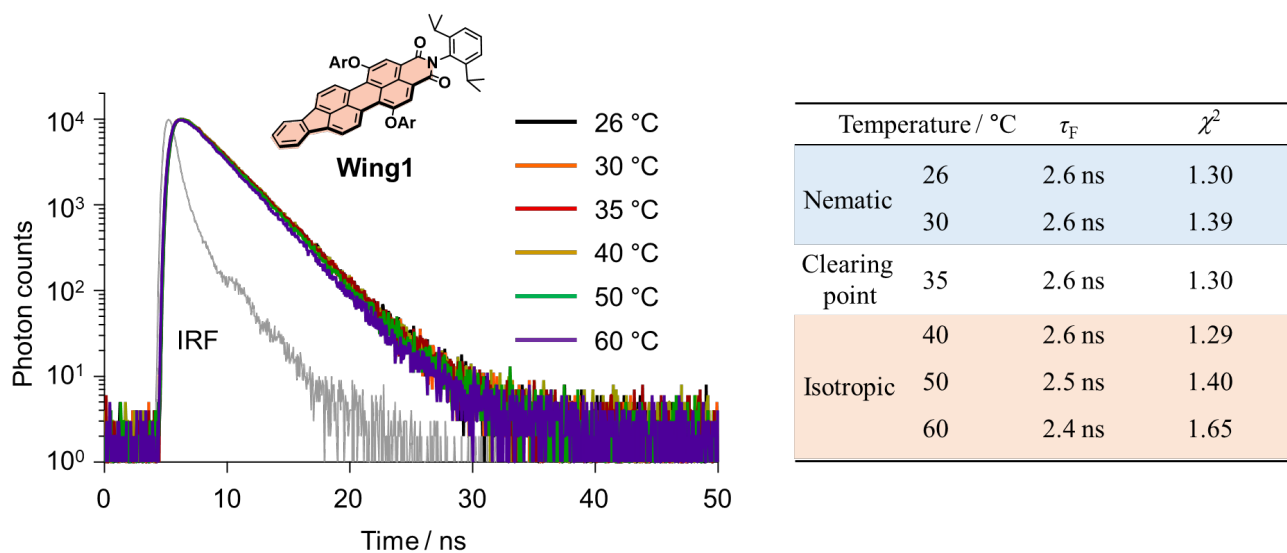
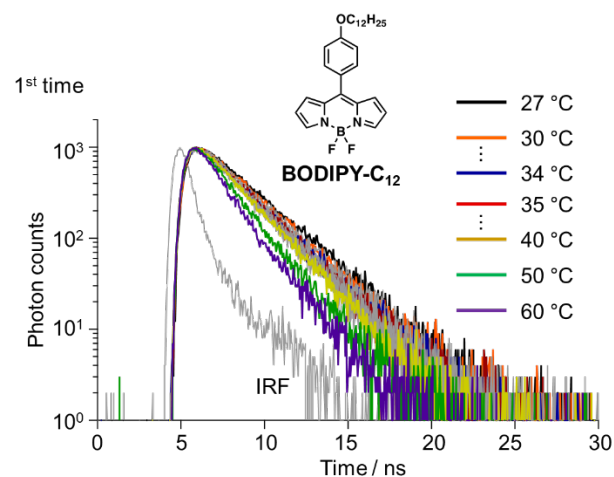
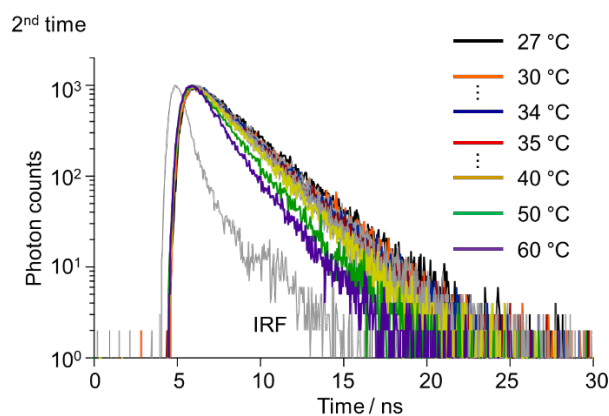


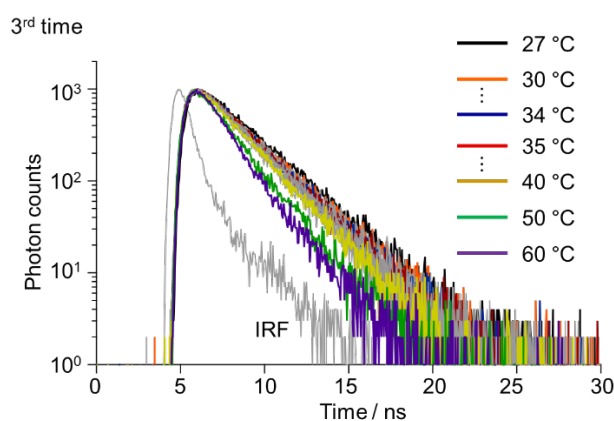
Figure S2-6. No temperature dependence of FL decay profiles and FL lifetimes of **Wing1** in 5CB ($\lambda_{\text{ex}} = 470$ nm and $\lambda_{\text{F}} = 582$ nm).



	Temperature / °C	τ_F	χ^2
Nematic	27	2.3 ns	1.11
	30	2.1 ns	1.00
	31	2.0 ns	1.15
	32	2.0 ns	1.28
	33	2.0 ns	1.26
	34	1.9 ns	1.33
	Clearing point	35	1.9 ns
Isotropic	36	1.9 ns	1.52
	37	1.8 ns	1.49
	38	1.8 ns	1.35
	39	1.8 ns	1.37
	40	1.8 ns	1.35
	60	1.1 ns	1.29



	Temperature / °C	τ_F	χ^2
Nematic	27	2.2 ns	1.10
	30	2.1 ns	1.46
	31	2.0 ns	1.10
	32	2.0 ns	1.39
	33	1.9 ns	1.24
	34	2.0 ns	1.16
	Clearing point	35	1.9 ns
Isotropic	36	1.9 ns	1.29
	37	1.8 ns	1.23
	38	1.8 ns	1.01
	39	1.7 ns	1.30
	40	1.8 ns	1.44
	60	1.4 ns	1.19



	Temperature / °C	τ_F	χ^2
Nematic	27	2.2 ns	1.22
	30	2.1 ns	1.34
	31	2.0 ns	1.40
	32	2.0 ns	1.16
	33	2.0 ns	1.30
	34	1.9 ns	1.39
	Clearing point	35	1.9 ns
Isotropic	36	1.9 ns	1.29
	37	1.8 ns	1.17
	38	1.8 ns	1.35
	39	1.7 ns	1.34
	40	1.7 ns	1.43
	60	1.4 ns	1.34

Figure S2-7. Temperature-dependent FL decay profiles and FL lifetimes of BODIPY-C₁₂ in 5CB ($\lambda_{\text{ex}} = 470$ nm and $\lambda_{\text{F}} = 520$ nm) for three measurements.

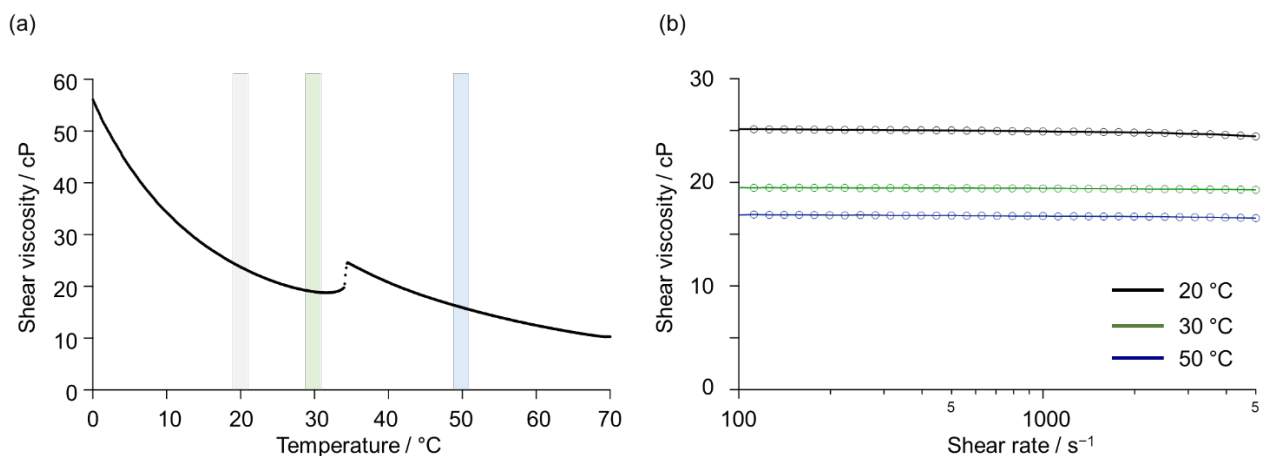


Figure S2-8. (a) Shear viscosity of 5CB measured by a rheometer (Shear rate: 500 s⁻¹, cooling rate: 6 °C min⁻¹). (b) Shear rate dependence of the shear viscosity of 5CB at each temperature (Shear rate: 100 to 5000 s⁻¹).

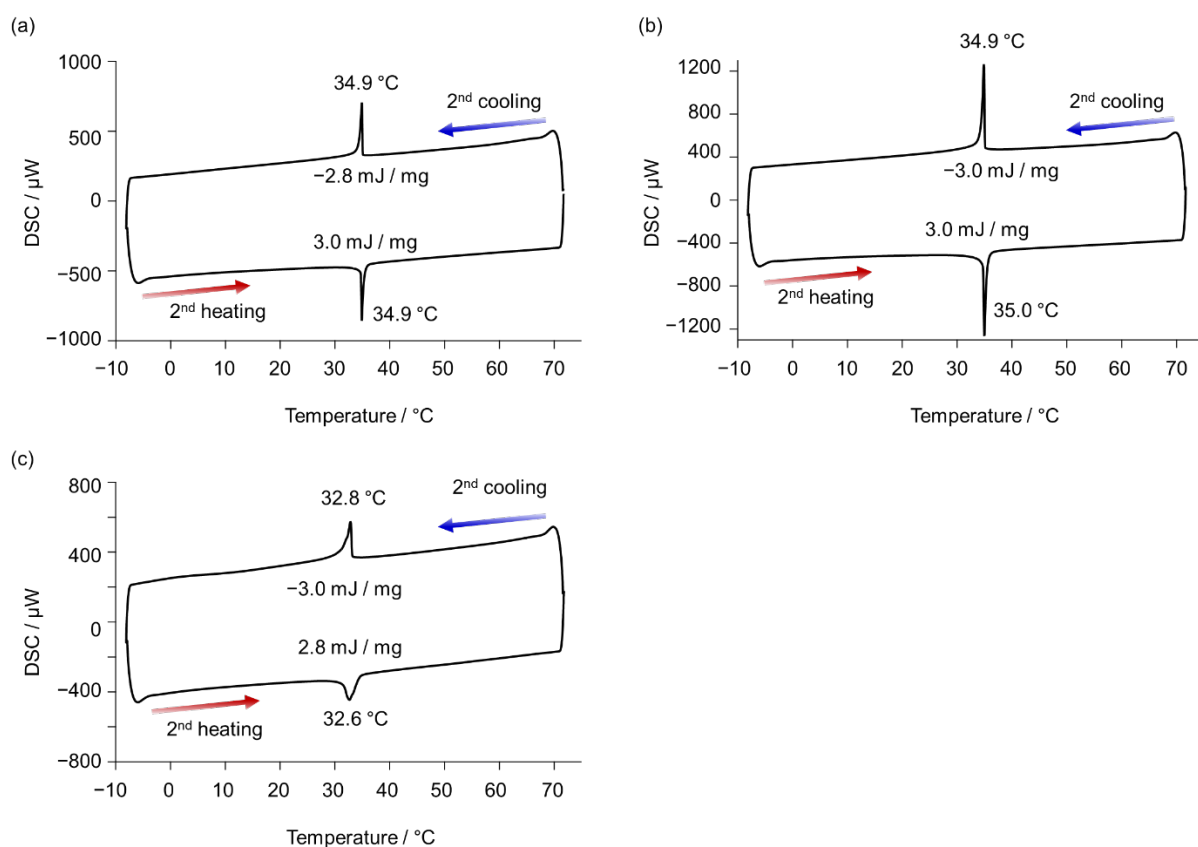


Figure S2-9. DSC analysis of (a) pure 5CB, (b) 5CB doped with **FLAP0** (0.01 wt%), and (c) 5CB doped with **FLAP0** (1 wt%).

Differential scanning calorimetry (DSC) measurements were conducted under N₂ atmosphere at a flow speed of 30 mL min⁻¹. Heating and cooling processes were shown in **Figure S2-10**. Each sample was placed in an aluminum pan and covered with an aluminum cover, which was pressed with a pressing tool. A vacant pan and a cover, which was also pressed, was used as a reference sample.

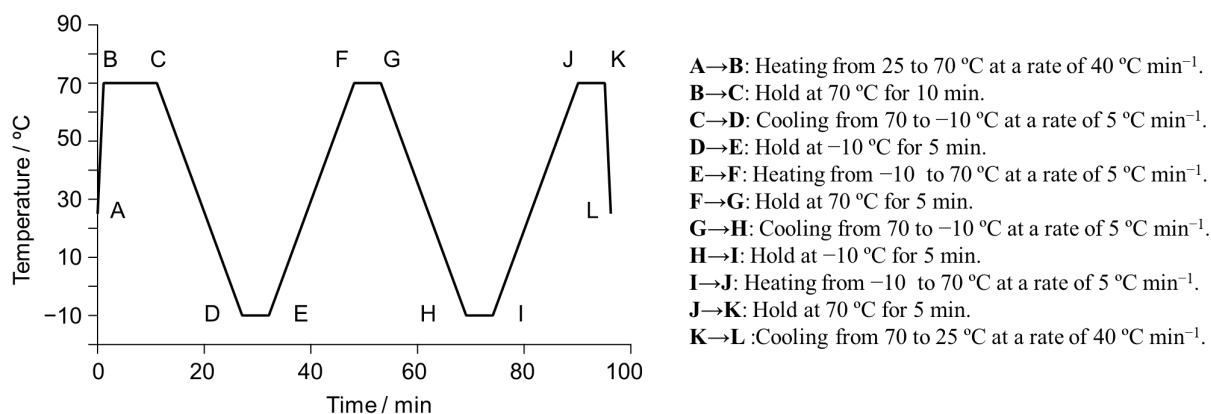
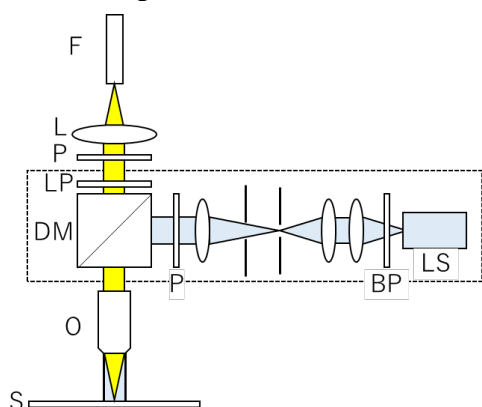


Figure S2-10. Heating and cooling processes of the DSC measurements.

3. Microscopic measurements



F: Fiber	BP: Band-pass filter
L: Lens	LS: Light-source (LED)
P: Polarizer	O: Objective
LP: Long-pass filter	S: Sample
DM: Dichroic mirror	

- Light Source: Thorlabs M385L2
- Bandpass filter : Nikon Bandpass 330-380
- Dichroic mirror : Semrock Di-405-25x36
- Longpass filter : Edmund OD4.0 Longpass450 nm
- UV Power: 80 μ W, spot size: \sim 340 μ m (23 mW/cm²)

Figure S3-1. Experimental setup and conditions of microscopic measurements. The polarizer in the detection path was inserted or removed as necessary. Measurements were made with typical illumination intensities of \sim 80 μ W over an illumination spot of \sim 340 μ m (corresponding to \sim 20 mW/cm²) and no photodegradation was observed during the measurements. For the analysis of the FL intensities at specified wavelengths, the intensities were extracted after applying binomial smoothing of 5 passes on the acquired spectra (performed using Igor Pro Software).

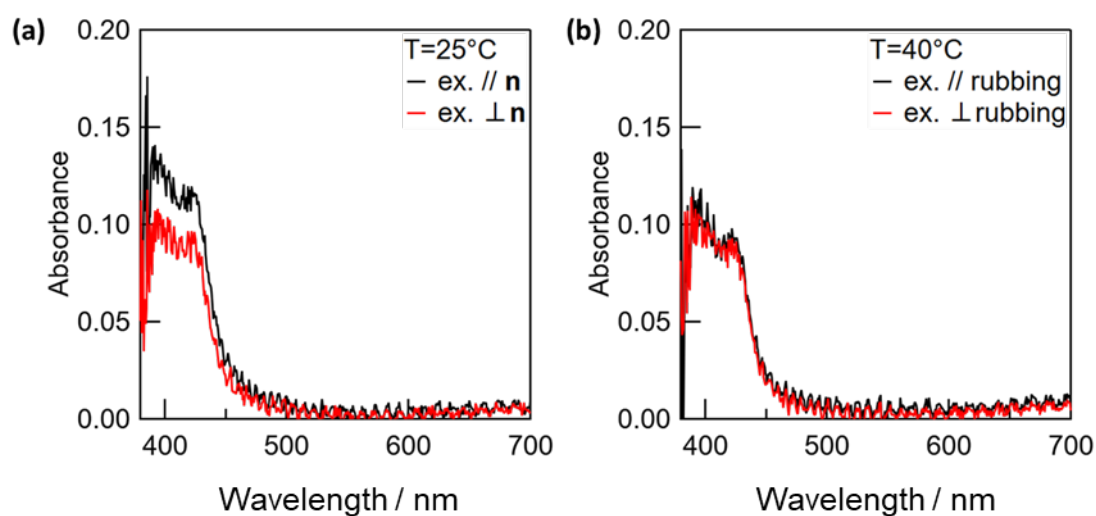


Figure S3-2. (a) Polarized absorbance spectra of **FLAP0** doped at a concentration of 1 wt% in 5CB, measured along (pol.//**n**) and perpendicular (pol.⊥**n**) to the director of 5CB in the nematic phase (25 °C). (b) Polarized absorbance spectra measured in the isotropic phase (40 °C), where the polarizations are written with reference to the rubbing axis on the substrate.

Note: We found that **FLAP0** doped in 5CB has a small anisotropy in the longer wavelength region of the absorption spectrum ($\lambda > 400$ nm), in which 5CB has no absorption, indicating that the ground-state direction of **FLAP0** is not completely isotropic.

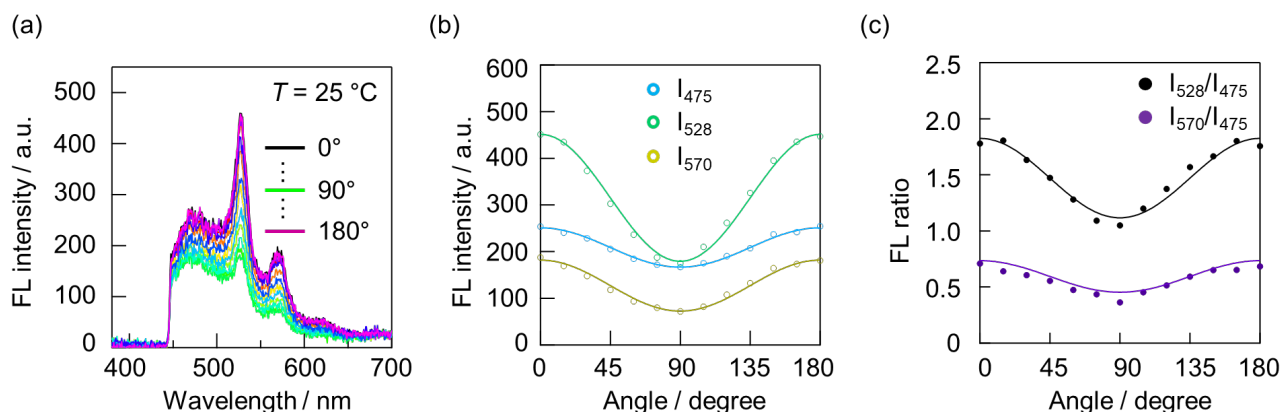


Figure S3-3. (a) Polarization-resolved FL spectra (non-polarized excitation, $\lambda_{\text{ex}} = 380$ nm) of **FLAP0** doped in 5CB (0.5 wt%) in the nematic phase (25 °C), where the polarization angle is measured from the director axis. (b) Dependence of the FL peak intensities on the polarizer angle. (c) Polarization dependence of the FL intensity ratios attributed to the planarized (528, 570 nm) and V-shaped (475 nm) **FLAP0** species in the S_1 excited state.

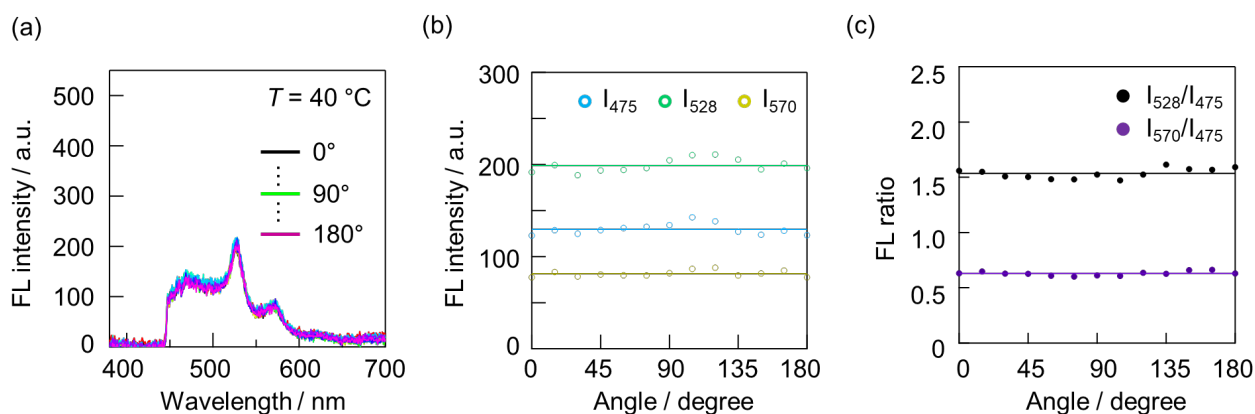


Figure S3-4. (a) Polarization-resolved FL spectra (non-polarized excitation, $\lambda_{\text{ex}} = 380$ nm) of **FLAP0** doped in 5CB (0.5%) in the isotropic phase (40 °C). The polarization angle is measured from the rubbing axis on the cell substrates. (b) Dependence of the FL peak intensities on the polarization angle. (c) Polarization dependence of the FL intensity ratios attributed to the planarized (528, 570 nm) and V-shaped (475 nm) **FLAP0** species in the S_1 excited state.

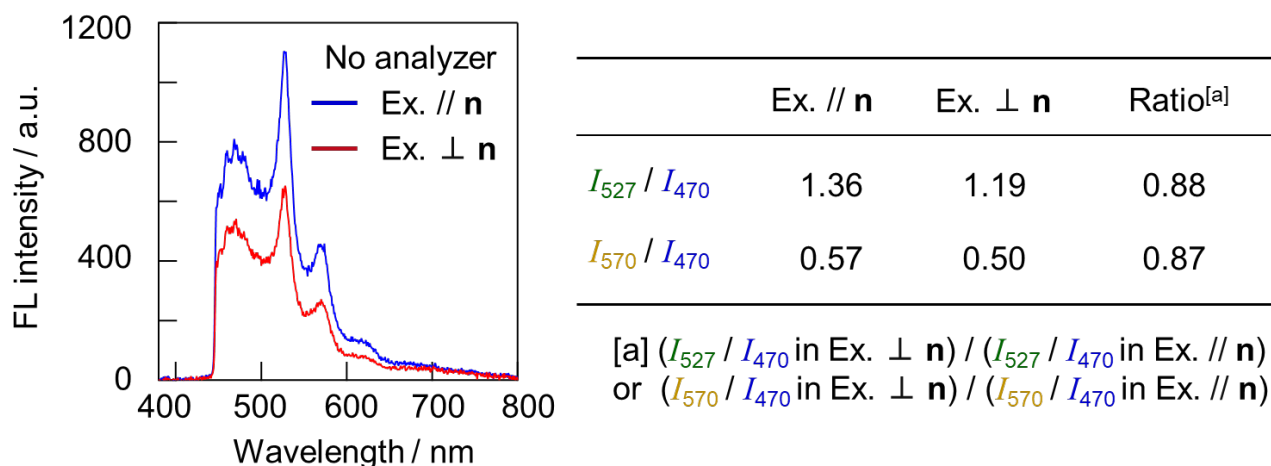


Figure S3-5. FL spectra and FL ratios of **FLAP0** in 5CB (0.5 wt%) at 25 °C excited with a polarized light ($\lambda_{\text{ex}} = 380$ nm) but detected with the analyzer removed. Ex.//**n** and Ex.⊥**n** indicate excitation polarizations parallel and perpendicular to the 5CB director, respectively.

Note: When **FLAP0** was excited with a polarized light and the FL was detected without an analyzer, the FL ratio showed a significant dependence on the polarization angle of the excitation light. This means that the degree of the suppression of the planarization dynamics is dependent on the direction of the V-shaped **FLAP0** in the ground state relative to the director of 5CB.

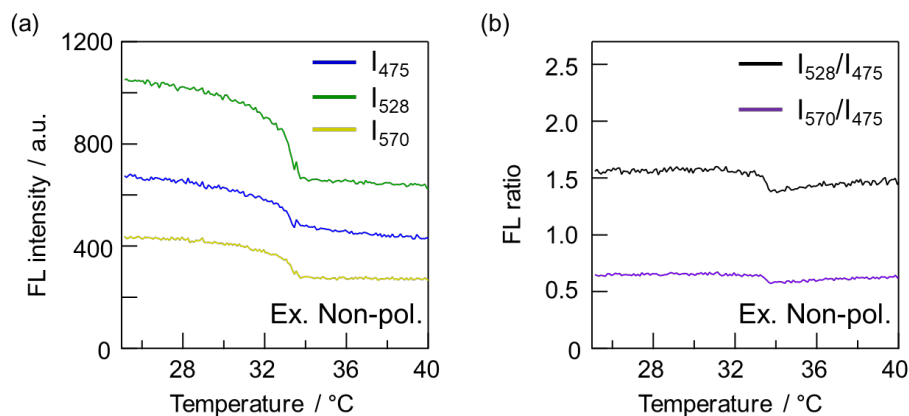


Figure S3-6. Temperature dependence of (a) the FL intensities and (b) the FL ratios of **FLAP0** doped in 5CB (0.5 wt%) excited with a non-polarized light ($\lambda_{\text{ex}} = 380$ nm) and detected without passing a polarizer. A kink is observed in the FL ratio at approx. 34 °C, demonstrating ratiometric detection of the phase transition by **FLAP0**.

4. Density functional theory (DFT) calculations

DFT calculations of the isolated molecules were performed using the Gaussian 16 program.^[S5] Kohn–Sham orbitals were displayed by the Avogadro program.^[S6] A model structure (**FLAP0'**) has hydrogen atoms in place of the 2,6-diisopropylphenyl groups of the corresponding molecule (**Figure S4-1**).

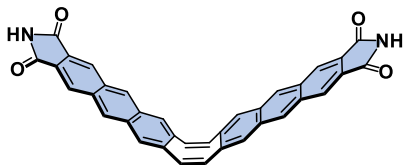


Figure S4-1. The model compound **FLAP0'** for the DFT calculations.

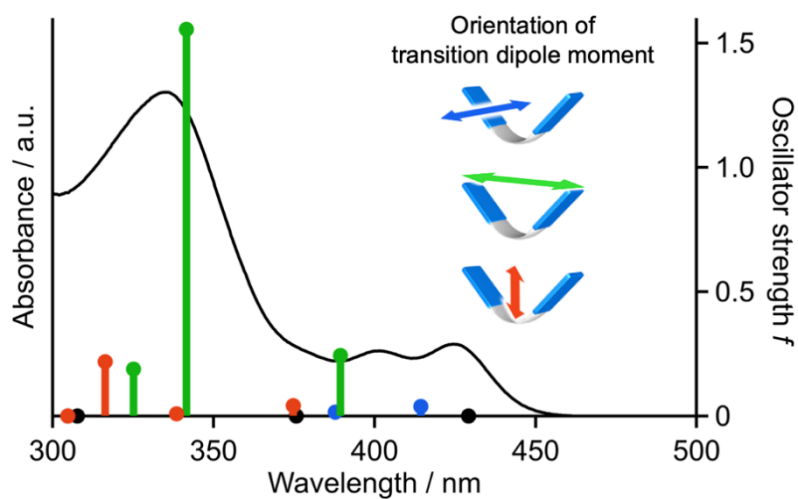
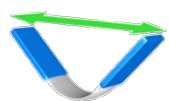
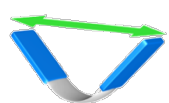


Figure S4-2. Oscillator strengths of $S_0 \rightarrow S_n$ transitions of **FLAP0'** (optimized geometry in S_0) calculated at the TD-PBE0/6-31+G(d) level (bars) and observed UV-visible absorption spectrum (line) of **FLAP0** in PhCN.

Table S4-1. Excitation energies and oscillator strengths for **FLAP0'** (optimized geometry in S_0) calculated at the TD-PBE0 /6-31+G(d) level.

Transition	Excitation energy	Configurations	f	Orientation of transition dipole moment
$S_0 \rightarrow S_1$	2.89 eV (429 nm)	HOMO \rightarrow LUMO (96%)	0	—
$S_0 \rightarrow S_2$	2.99 eV (414 nm)	HOMO \rightarrow LUMO+1 (92%)	0.0382	
		HOMO-1 \rightarrow LUMO (7%)		
$S_0 \rightarrow S_3$	3.18 eV (389 nm)	HOMO \rightarrow LUMO+2 (70%)	0.2438	
		HOMO-2 \rightarrow LUMO (16%)		
		HOMO-1 \rightarrow LUMO+3 (8%)		
$S_0 \rightarrow S_4$	3.20 eV (388 nm)	HOMO-1 \rightarrow LUMO (92%)	0.0153	
		HOMO \rightarrow LUMO+1 (7%)		
$S_0 \rightarrow S_5$	3.30 eV (376 nm)	HOMO-1 \rightarrow LUMO+1 (96%)	0	—
$S_0 \rightarrow S_6$	3.31 eV (375 nm)	HOMO \rightarrow LUMO+3 (37%)	0.0421	
		HOMO-1 \rightarrow LUMO+2 (29%)		
		HOMO-2 \rightarrow LUMO+1 (24%)		
$S_0 \rightarrow S_7$	3.63 eV (342 nm)	HOMO-2 \rightarrow LUMO (75%)	1.5553	
		HOMO \rightarrow LUMO+2 (22%)		
$S_0 \rightarrow S_8$	3.66 eV (339 nm)	HOMO \rightarrow LUMO+3 (53%)	0.0089	
		HOMO-1 \rightarrow LUMO+2 (41%)		

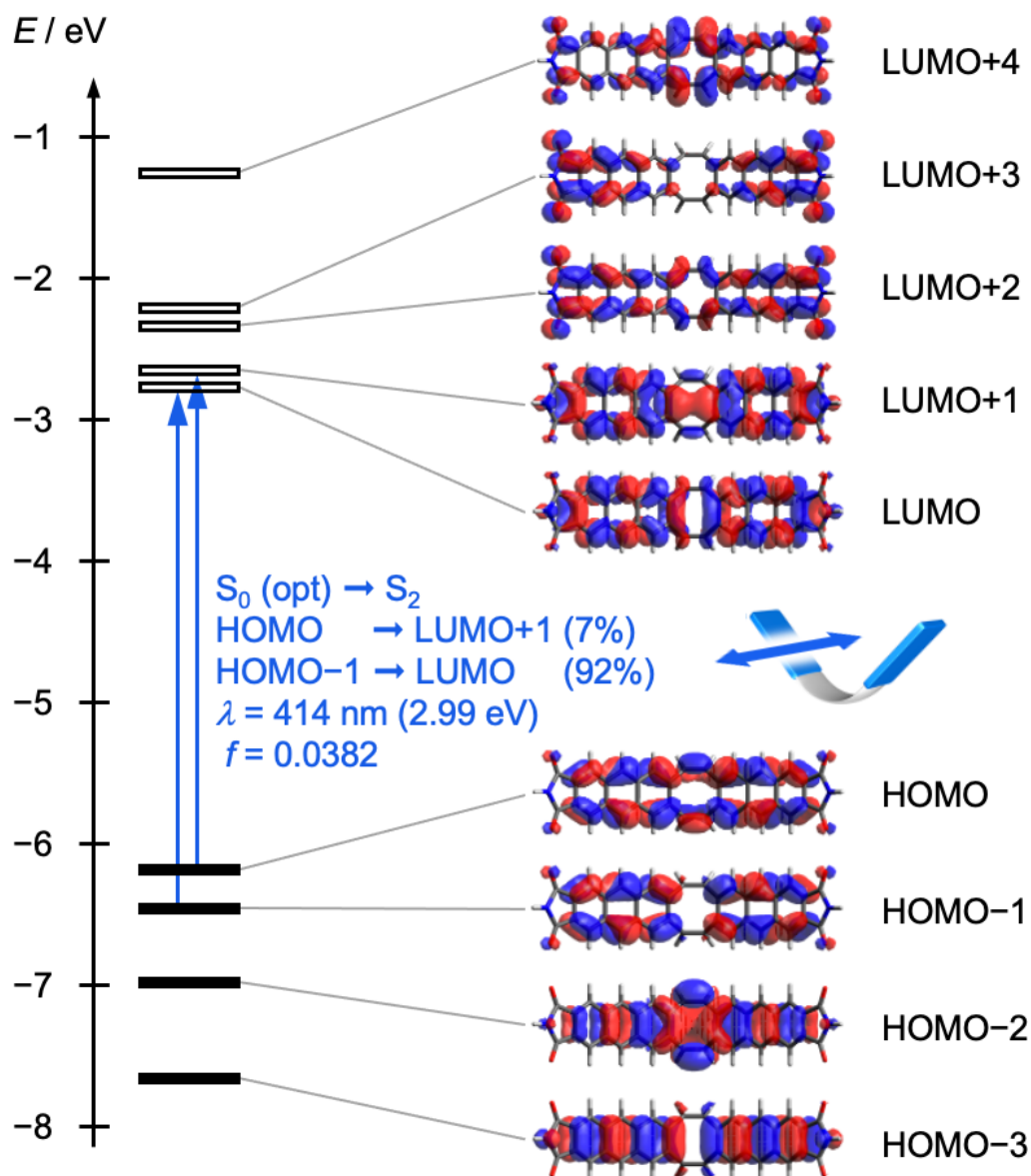


Figure S4-3. Kohn–Sham molecular orbitals of **FLAP0'** in the S_0 optimized geometry (C_{2v} symmetry, COT bending angle $\theta = 41.1^\circ$) and the transition character of the absorption in the longest wavelength region, calculated at the (TD-)PBE0/6-31+G(d) level. See the reference [S2] for the definition of the COT bending angle.

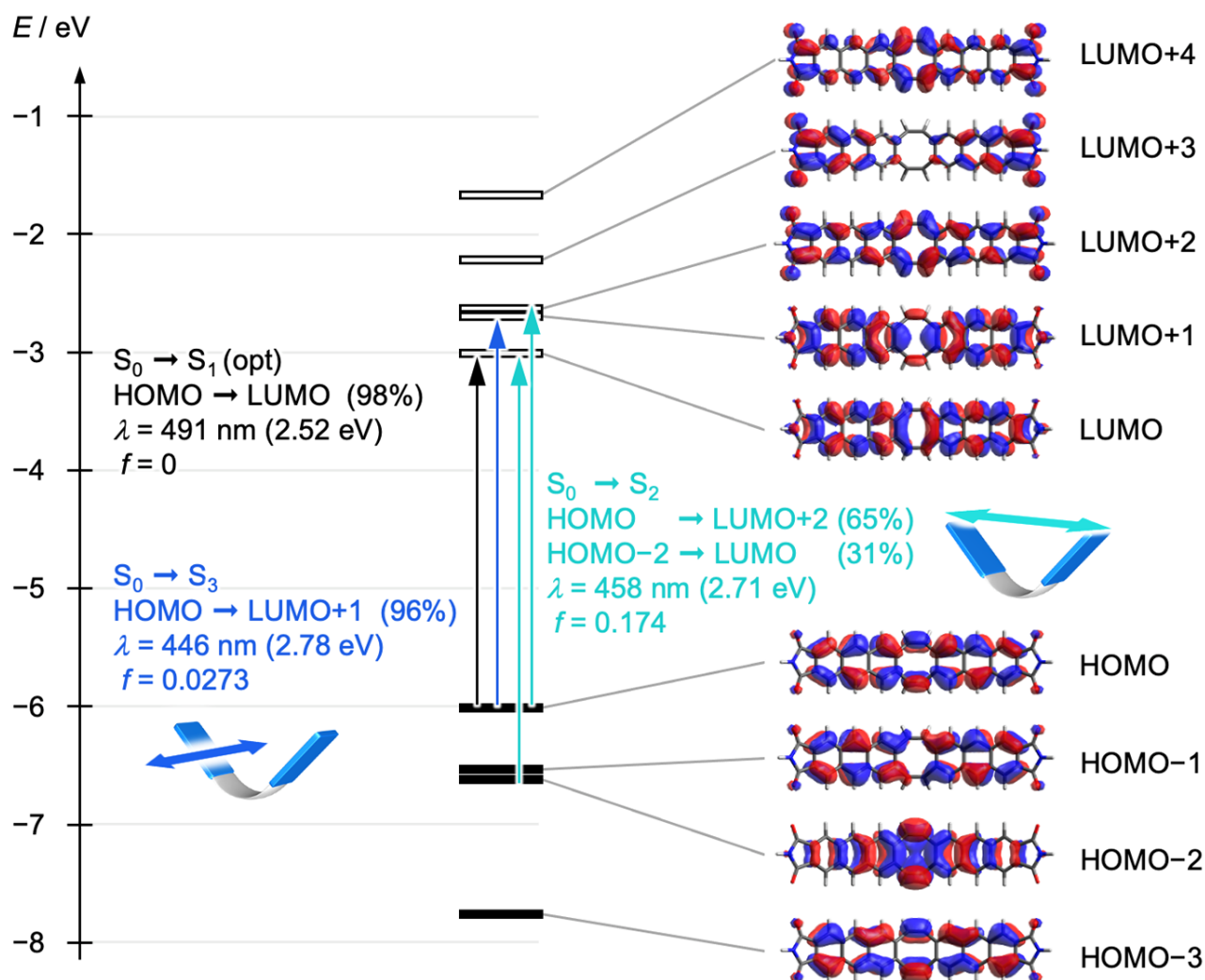


Figure S4-4. Kohn–Sham molecular orbitals of **FLAP0'** with the shallow V-shaped structure (C_{2v} symmetry) at the S_1 local minimum (COT bending angle $\theta = 28.2^\circ$) and the transition characters, calculated at the TD-PBE0/6-31+G(d) level. See the reference [S2] for the definition of the COT bending angle.

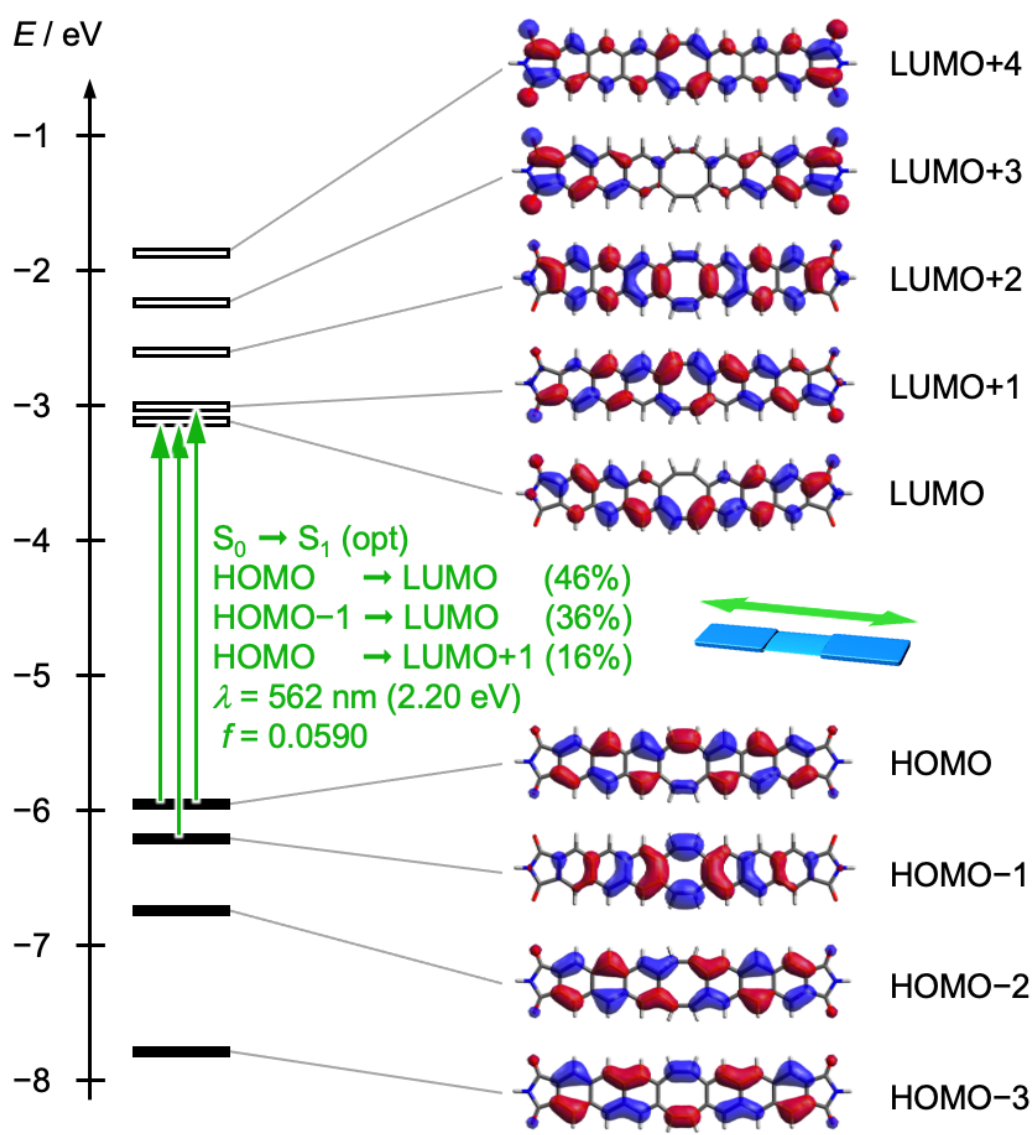


Figure S4-5. Kohn–Sham molecular orbitals of FLAP0' with the planar structure (C_{2v} symmetry) at the S_1 global minimum (COT bending angle $\theta = 0^\circ$) and the transition character of the fluorescence, calculated at the TD-PBE0/6-31+G(d) level. See the reference [S2] for the definition of the COT bending angle.

5. Supporting references

- S1. R. Kotani, H. Sotome, H. Okajima, S. Yokoyama, Y. Nakaike, A. Kashiwagi, C. Mori, Y. Nakada, S. Yamaguchi, A. Osuka, A. Sakamoto, H. Miyasaka and S. Saito, *J. Mater. Chem. C* **2017**, *5*, 5248.
- S2. R. Kimura, H. Kuramochi, P. Liu, T. Yamakado, A. Osuka, T. Tahara and S. Saito, *Angew. Chem. Int. Ed.* **2020**, *59*, 16430.
- S3. M. K. Kuimova, G. Yahioğlu, J. A. Levitt and K. Suhling, *J. Am. Chem. Soc.* **2008**, *130*, 6672.
- S4. W. Nakanishi, S. Saito, N. Sakamoto, A. Kashiwagi, S. Yamaguchi, H. Sakai and K. Ariga, *Chem. Asian J.* **2019**, *14*, 2869.
- S5. Gaussian 16, Revision A.03, M. J. Frisch, G. W. Trucks, H. B. Schlegel, G. E. Scuseria, M. A. Robb, J. R. Cheeseman, G. Scalmani, V. Barone, G. A. Petersson, H. Nakatsuji, X. Li, M. Caricato, A. V. Marenich, J. Bloino, B. G. Janesko, R. Gomperts, B. Mennucci, H. P. Hratchian, J. V. Ortiz, A. F. Izmaylov, J. L. Sonnenberg, D. Williams-Young, F. Ding, F. Lipparini, F. Egidi, J. Goings, B. Peng, A. Petrone, T. Henderson, D. Ranasinghe, V. G. Zakrzewski, J. Gao, N. Rega, G. Zheng, W. Liang, M. Hada, M. Ehara, K. Toyota, R. Fukuda, J. Hasegawa, M. Ishida, T. Nakajima, Y. Honda, O. Kitao, H. Nakai, T. Vreven, K. Throssell, J. A. Montgomery, Jr., J. E. Peralta, F. Ogliaro, M. J. Bearpark, J. J. Heyd, E. N. Brothers, K. N. Kudin, V. N. Staroverov, T. A. Keith, R. Kobayashi, J. Normand, K. Raghavachari, A. P. Rendell, J. C. Burant, S. S. Iyengar, J. Tomasi, M. Cossi, J. M. Millam, M. Klene, C. Adamo, R. Cammi, J. W. Ochterski, R. L. Martin, K. Morokuma, O. Farkas, J. B. Foresman, and D. J. Fox, Gaussian, Inc., Wallingford CT, **2016**.
- S6. M. D. Hanwell, D. E. Curtis, D. C. Lonie, T. Vandermeersch, E. Zurek and G. R. Hutchison, *J. Cheminformatics* **2012**, *4*, 17.